remote sensing

MDPI

Article

Atmospheric Trace Gas (NO_2 and O_3) Variability in South Korean Coastal Waters, and Implications for Remote Sensing of Coastal Ocean Color Dynamics

Maria Tzortziou [1,2,*], Owen Parker [1], Brian Lamb [1], Jay R. Herman [2,3], Lok Lamsal [2,4], Ryan Stauffer [2,4] and Nader Abuhassan [2,3]

1 Department of Earth and Atmospheric Sciences, The City College of New York, City University of New York, New York, NY 10031, USA; owparker@gmail.com (O.P.); blamb25@gmail.com (B.L.)
2 NASA Goddard Space Flight Center, Greenbelt, MD 20771, USA; jay.r.herman@nasa.gov (J.R.H.); lok.lamsal@nasa.gov (L.L.); ryan.m.stauffer@nasa.gov (R.S.); nader.abuhassan@nasa.gov (N.A.)
3 Joint Center for Earth Systems Technology, University of Maryland, Baltimore, MD 21201, USA
4 Goddard Earth Sciences Technology and Research, Universities Space Research Association, Columbia, MD 21046, USA
* Correspondence: mtzortziou@ccny.cuny.edu; Tel.: +1-212-650-5769

Received: 13 September 2018; Accepted: 1 October 2018; Published: 3 October 2018

Abstract: Coastal environments are highly dynamic, and are characterized by short-term, local-scale variability in atmospheric and oceanic processes. Yet, high-frequency measurements of atmospheric composition, and particularly nitrogen dioxide (NO_2) and ozone (O_3) dynamics, are scarce over the ocean, introducing uncertainties in satellite retrievals of coastal ocean biogeochemistry and ecology. Combining measurements from different platforms, the Korea-US Ocean Color and Air Quality field campaign provided a unique opportunity to capture, for the first time, the strong spatial dynamics and diurnal variability in total column (TC) NO_2 and O_3 over the coastal waters of South Korea. Measurements were conducted using a shipboard Pandora Spectrometer Instrument specifically designed to collect accurate, high-frequency observations from a research vessel, and were combined with ground-based observations at coastal land sites, synoptic satellite imagery, and air-mass trajectory simulations to assess source contributions to atmospheric pollution over the coastal ocean. TCO_3 showed only small (<20%) variability that was driven primarily by larger-scale meteorological processes captured successfully in the relatively coarse satellite imagery from Aura-OMI. In contrast, $TCNO_2$ over the ocean varied by more than an order of magnitude (0.07–0.92 DU), mostly affected by urban emissions and highly dynamic air mass transport pathways. Diurnal patterns varied widely across the ocean domain, with $TCNO_2$ in the coastal area of Geoje and offshore Seoul varying by more than 0.6 DU and 0.4 DU, respectively, over a period of less than 3 h. On a polar orbit, Aura-OMI is not capable of detecting these short-term changes in $TCNO_2$. If unaccounted for in atmospheric correction retrievals of ocean color, the observed variability in $TCNO_2$ would be misinterpreted as a change in ocean remote sensing reflectance, R_{rs}, by more than 80% and 40% at 412 and 443 nm, respectively, introducing a significant false variability in retrievals of coastal ocean ecological processes from space.

Keywords: ocean color; satellite; atmospheric variability; nitrogen dioxide; ozone; coastal; ecology; biogeochemistry

1. Introduction

At the interface between the land, oceans, and atmosphere, coastal regions are highly dynamic environments, characterized by strong variability in both water and air quality. Variability in atmospheric composition is associated with short-term (e.g., hourly) changes and periodic (e.g., weekly)

patterns in anthropogenic emissions, as well as complex meteorological processes that influence the circulation and accumulation of atmospheric pollutants at land-water boundaries [1–3]. Previous studies, using high spatial resolution meteorological and air quality simulations covering the Chesapeake Bay and adjacent Atlantic Ocean coastline, have demonstrated that air pollution from coastal urban areas often accumulates over adjacent coastal waters due to low dry deposition rates over the water and a shallow marine boundary layer that traps marine emissions [3,4]. Local-scale meteorological processes, such as sea- and bay-breeze circulations, further affect the advection, recirculation, and accumulation of atmospheric pollutants in coastal areas, often leading to a build up of emissions and aggravation of air pollution along the shoreline caused by stagnation that develops as wind directions change [4–8]. Strong, prolonged sea or bay breeze events can transport a large amount of urban air pollution out of the planetary boundary layer and into the free troposphere, where pollutants have longer lifetimes and are susceptible to long range transport offshore and over adjacent ocean environments, with potentially significant ecological impacts for aquatic ecosystems [9].

Assessing the spatial and temporal variability of atmospheric pollutants, aerosols, and absorbing trace gases in coastal areas is critical for improving modeling and prediction of coastal tropospheric air quality, determining impacts on human health, and assessing the ecological implications of atmospheric pollutant deposition in coastal ecosystems [4]. It is also essential not only for improved satellite trace gas retrievals, but also for accurate atmospheric correction of satellite coastal ocean color observations, especially in coastal waters that are close to heavily polluted urban areas [2,10,11]. If not adequately corrected, this atmospheric variability can lead to a false estimate of time-dependent underwater processes from a satellite ocean color sensors. The errors can be aliased as day-to-day or weekly variability in retrievals from polar orbiting sensors, such as MODIS, VIIRS, PACE, and OLCI, impacting their ability to monitor the evolution of marine biological processes such as algal blooms. They can also introduce a false diurnal variability in ocean retrievals from geostationary sensors such as GOCI [12,13].

Ozone (O_3) and nitrogen dioxide (NO_2) in the atmosphere have absorption bands in ultraviolet, visible, and near-infrared wavelengths relevant to ocean color remote sensing [14]. NO_2 absorption peaks at 400-445 nm, affecting the top of atmosphere (TOA) signal measured by an ocean color satellite sensor at wavelengths traditionally used for retrievals of phytoplankton pigments and dissolved organic carbon dynamics [15–18]. Radiative transfer calculations by Tzortziou et al. [19] showed that 0.7 DU unaccounted variability in NO_2, which is consistent with the NO_2 variability previously measured over coastal areas often covered by just a single early afternoon OMI pixel [7], results in a level of uncertainty in coastal water remote sensing reflectance, R_{rs}, which may be as large as 40% at 412 nm, for low solar zenith angles (SZA < 30°), and NO_2 distributed within the first 2 km from the ground. This error increases with decreasing wavelength, increasing solar and satellite viewing angles, and as the NO_2 is distributed at higher altitudes, reaching up to 80% or more for SZAs expected with a geostationary sensor [10,19]. The resulting errors in R_{rs} absolute magnitude and spectral shape subsequently introduce significant and time-dependent uncertainties in retrievals of ocean biogeochemical variables from space [10,13,19,20].

Satellite observations provide a powerful tool for assessing O_3 and NO_2 emissions, distribution, and transport over land and the ocean. To enhance the scientific return of satellite remote sensing, obtain a more complete picture of the atmosphere, and increase our understanding of the effects of air pollution on coastal ecosystem dynamics, satellite observations must be used in combination with model simulations and detailed measurements from surface platforms. This becomes extremely challenging in coastal regions, since ground-based networks that monitor tropospheric air quality abruptly end at the coastlines. Previous studies integrating high frequency observations to assess the impact of atmospheric trace gas variability on ocean color retrievals were based on measurements at coastal sites over the land [10,19]. This paper specifically addresses this challenge by quantifying, for the first time, atmospheric variability of NO_2 and O_3 in the coastal waters of South Korea, measured from a shipboard Pandora Spectrometer Instrument (PSI) specifically designed to collect accurate, high-frequency, direct-sun observations from a moving platform. Measurements were collected from

the research vessel (RV) *Onnuri* during the 2016 Korean and US Ocean Color and Air Quality (KORUS OC/AQ) field campaign.

South Korea is embedded in a region of increasing economic change with strong gradients in air quality in time and space [21]. Rapid industrialization, increasing coastal urbanization, and weak regulation of local anthropogenic emissions have caused serious air pollution problems in the region, which are often severely aggravated by long range transport of pollutants. Dramatic increases in NO_x emissions have been observed over eastern Asia since 2000 [22–24], posing major threats to both human health and downwind terrestrial and ocean ecosystems. Our high frequency measurements from RV *Onnuri* during KORUS OC/AQ captured, for the first time, the strong spatial dynamics and diurnal variability in total column atmospheric NO_2 and O_3 over the coastal waters of South Korea. In this study, shipboard observations over the ocean are integrated with ground-based observations at coastal land sites to examine differences across the land-ocean interface, and are combined with air-parcel back-trajectory simulations to assess source contributions to atmospheric pollution over these coastal waters. Comparisons of surface measurements with satellite Aura-OMI retrievals of O_3 and NO_2 reveal the capabilities and limitations of coarse resolution, polar-orbiting satellite observations in capturing variability in atmospheric pollution gradients over terrestrial-aquatic interfaces, and the need for concurrent measurements of NO_2 and O_3 to obtain accurate corrections of coastal ocean color satellite imagery in highly polluted coastal urban regions.

2. Methods

2.1. Study Region

The Korea-United States Ocean Color (KORUS-OC) expedition was an 18-day oceanographic field campaign conducted from 20 May to 6 June 2016 in the East Sea and Yellow Sea, under the leadership of the Korean Institute of Ocean Science and Technology (KIOST) and the United States National Aeronautics and Space Administration (NASA) [25]. KORUS OC was coordinated with the Korea-United States Air Quality (KORUS-AQ) study, led by Korea's National Institute of Environmental Research (NIER) and NASA [21]. The overarching objectives of these coordinated campaigns were to improve our understanding of the factors contributing to poor air quality in Korea, characterize highly dynamic biological and biogeochemical processes in coastal waters, and capture diurnal variability in biology, biogeochemistry, atmospheric properties and physics to enable improved capabilities for satellite remote sensing and model simulation of atmospheric composition, ocean biology, and biogeochemistry. One of the main goals of these studies was to perform ocean and atmospheric measurements for risk reduction of future satellite observations from geostationary platforms, in an area that is within the field-of-view of the only available geostationary Ocean Color instrument: the Korean GOCI (Geostationary Ocean Color Imager) sensor.

The coastal waters of the Yellow Sea and East Sea/Sea of Japan are strongly impacted by both local atmospheric pollution and the long-range transport of air pollutants from other highly polluted urban centers in East Asia, including Shanghai and Beijing [26,27]. Yet, the impacts of atmospheric pollutants on sea-air exchanges and coastal ocean color retrievals remain largely unknown. Using observations from different platforms, including aircraft, ground sites, and research vessels, the KORUS-OC/AQ study provided unprecedented comprehensive measurements of pollutants (both trace gases and aerosol particle properties) with extensive spatial and vertical coverage. Here, we focus on the spatial and temporal variability of total column NO_2 and O_3 measured by the shipboard NASA PSI-24, operating in direct-sun mode. The spectrometer was mounted on the 1422-ton RV *Onnuri*, one of the Korean Ocean Research and Development Institute (KORDI)'s research vessels.

During the KORUS OC campaign, the RV *Onnuri* covered an area along the Eastern, Southern, and Western South Korean coasts (Figure 1). Measurements in South Korean territorial waters are excluded by international agreement from this study. The RV *Onnuri* departed from the KIOST South Sea Research Institute dock at Geoje, near the Busan metropolitan area, on 20 May, sailing North-East

into the Sea of Japan, and looped around Ullung-do ("do" means island). Its maximum northerly extent was 37.87° latitude, and its maximum easterly extent was 131.38° longitude (23 May 2016). It then navigated along the east coast of the Korean Peninsula, examining the region near the industrial center of Pohang (27 May 2016), passed south of the Korean coast (maximum southerly extent 33.78° latitude on 28 May 2016), and then rounded the Jeollanam-do province of the southern Korean Peninsula, and proceeded North-West, transiting between the Heuksan-do and Hong-do (29 May 2016) and surveying the region west of Gwangju (maximum westerly extent 124.32° longitude on 30 May 2016). From there, the RV *Onnuri* first went northward, until it was off the western coast of the Seoul capital region (01 June 2016). The ship then headed back South-West, and then East to the KIOST South Sea Research Institute dock on 6 June 2016. Measurements from the shipboard Pandora Spectrometer Instrument (PSI-24) were collected from 18 to 20 May at the coastal site of Geoje, more than 35 km from the city of Busan, and over the ocean from 20 May to 2 June 2016 (cloud conditions during 3–6 June prevented direct-sun observations) (Figure 1). These shipboard measurements were compared to measurements from ground-based PSIs to assess differences in total column amounts of NO_2 and O_3 over the land and over the coastal ocean (Table 1; Figure 1). Ground sites included both heavily-polluted urban areas (e.g., Seoul and Busan) affected by anthropogenic emissions, as well as relatively less polluted, rural areas (e.g., Gwangju and Anmyeon) [28].

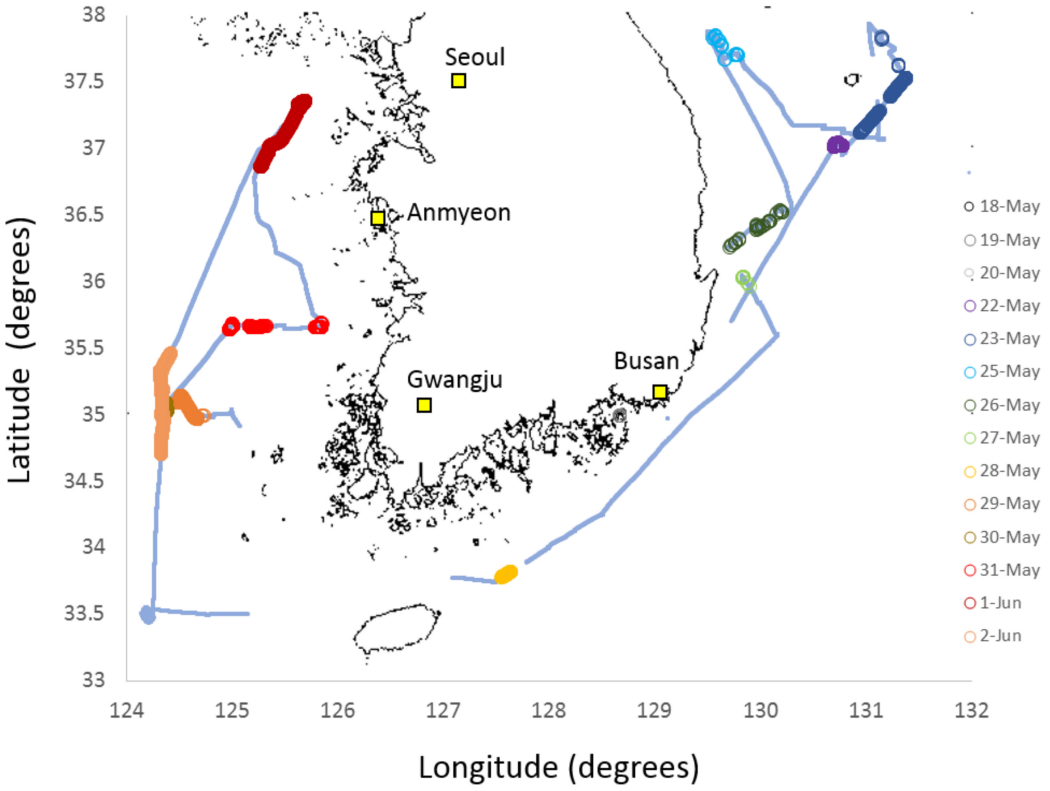

Figure 1. Map with the RV *Onnuri* tracks during the 2016 KORUS OC/AQ field campaign. Measurements in the South Korean territorial waters are excluded from this study.

Table 1. Locations of coastal ground-based PSI sites during KORUS-AQ.

Location	Lat	Lon	PSI	Measurement Period
Busan	35.24°	129.08°	PSI-17	07 April 2016–03 October 2016
Gwangju	35.23°	126.84°	PSI-26	01 May 2015–17 October 2016
Anmyeon	36.54°	126.33°	PSI-19	01 May 2016–06 June 2016
Seoul	37.56°	126.93°	PSI-40	16 May 2016–15 October 2016

2.2. Measurements of Total Column Trace Gases

Pandora Spectrometer Instrument (PSI) retrievals: A direct-sun PSI [1,11], modified for shipboard deployment, was used to measure total vertical column density of NO_2 ($TCNO_2$) and ozone (TCO_3). The Pandora system consists of a small Avantes low stray light spectrometer (spectral range: 280–525 nm; spectral resolution: 0.6 nm with 4 times oversampling) connected to an optical head by a 400 micron single strand fiber optic cable. The spectrometer is temperature stabilized at 20 °C inside two weather resistant containers [28]. The head sensor is mounted on two computer-controlled motors to control the azimuth and zenith viewing angles to ±0.01°. For the shipboard PSI, the Blick Software suite operating the PSI uses feedback from an internal digital camera to a sun-tracker to adjust the motors and maintain a centered direct-sun view. During KORUS-OC, Pandora was mounted on the bow/forecastle deck of the RV *Onnuri*, away from the ship engine's exhaust, to avoid any obstructions and contamination. Results from an instrument inter-comparison, using the 11 different PSIs that were deployed during the DISCOVER-AQ (Deriving Information on Surface Conditions from COlumn and VERtically Resolved Observations Relevant to Air Quality) field campaign in the Chesapeake Bay, showed excellent agreement among the instruments: differences were within ±4.8 DU (or ±1.5%) for TCO_3 and ±0.07 DU for $TCNO_2$, with no air-mass-factor dependence [2]. A similar result was shown for NO_2 from two PSIs deployed during the KORUS-AQ campaign [28].

Pandora TCO_3 and $TCNO_2$ amounts are determined using the Differential Optical Absorption Spectroscopy (DOAS) method. The spectral fitting algorithm uses laboratory-measured absorption cross sections for each atmospheric absorber, a 4th order polynomial in wavelength to remove aerosols and Rayleigh scattering effects, and wavelength shift and squeeze functions to remove wavelength errors at the 1 picometer level. The shift and squeeze functions provide the best match to the measured spectrum compared to a solar reference spectrum containing the solar Fraunhofer line structure [1,11]. PSI data were filtered following Tzortziou et al. [2] for a normalized root-mean-square of the weighted spectral fittings of <0.05, SZAs < 70°, and for uncertainties less than 0.05 DU for $TCNO_2$ and less than 2 DU for TCO_3.

OMI retrievals: The Ozone Monitoring Instrument (OMI), launched on NASA's Earth Observing System Aura satellite on July 15, 2004, has been collecting data since 9 August 2004 [29]. Aura has a sun-synchronous polar orbit at approximately 705 km altitude with a period of 100 min and a local equator crossing time between 13:40 and 13:50 local time. OMI is a UV/Visible grating imaging spectrometer that provides near-global coverage in one day. The size of an OMI pixel varies with cross-track viewing zenith angle from 24 km in the nadir to almost 128 km for the extreme viewing angles of 57° at the edges of the swath [30]. OMI measurements cover a spectral region of 264–504 nm with a spectral resolution between 0.42 nm and 0.63 nm, and provide retrievals for a number of trace gases including O_3, NO_2, SO_2, HCHO, BrO, and OClO.

PSI results are compared here with most recent versions of OMI $TCNO_2$, and TCO_3 station overpass data (OMNO2 product, Collection 3.0, Version 3.1; and OMTO3, Collection 3.0, Version 8.5 overpass products; http://avdc.gsfc.nasa.gov/index.php?site=1593048672&id=28) for the four coastal ground-based PSI sites Busan, Gwangju, Anmyeon and Seoul (Table 1). OMI station overpass data files provide the nearest OMI measurement in an OMI track (orbit), if it is closer than 100 km, to the ground-station. For comparison with the shipboard PSI measurements on RV *Onnuri*, match ups were created based on collocation such that the location of the ship was within the OMI pixel [31]. The maximum collocation distance between the center of the OMI FOV and the PSI location was 26 km for the NO_2 retrievals and 42 km for the O_3 retrievals. OMI data were not available during our shipboard measurements from 30 May to 2 June 2016 as the instrument went into survival mode on 29 May and resumed taking measurements on 10 June 2016. We used OMI measurements during clear-sky conditions (cloud fraction < 0.3) and excluded the data affected by Row Anomaly [32].

2.3. HYSPLIT Trajectory Generation

The NOAA Air Resources Laboratory's (ARL's) HYbrid Single-Particle Lagrangian Integrated Trajectory (HYSPLIT4) modeling system [33,34] was used to compute air parcel trajectories and determine the origin of air masses sampled by the shipboard PSI-24 on RV *Onnuri* during KORUS OC. HYSPLIT has been used extensively in the literature in a variety of applications to simulate the atmospheric transport, dispersion, and deposition of pollutants and hazardous materials [35–38]. HYSPLIT simulations were run using meteorological data from the Global Data Assimilation System (GDAS1.0), because the complex terrain of the Korean Peninsula necessitated favoring a data-set which allowed for the most representative modeling of vertical motion [39]. A previous comparison of HYSPLIT backward trajectories generated from both GDAS1.0 and GDAS0P5 datasets in the nearby Pearl River Delta reported that trajectories produced using GDAS1.0 showed better agreement with observations due to the absence of vertical velocity in GDAS0P5 dataset [40]. Thus, GDAS1.0 datasets were used in modeling trajectories in our study, while GDAS0.5 datasets were used to confirm the general direction of the trajectory. Results are shown here for the RV *Onnuri* measurements at Geoje and offshore the coastal sites of Gwangju, Anmyeon and Seoul. Backward trajectories were initialized at 1500 m AGL (above ground level) to examine air mass transport and origin at an altitude over the research vessel where NO_2 changes have a considerable impact on atmospheric correction of ocean color retrievals [1,19]. To check for errors in modeling, forward and back trajectories were created for each observation [39]. The termination point for each backward trajectory was used to produce a forward trajectory. All points along the two trajectories were then compared, with differences in excess of 10 km resulting in trajectory disposal and flagging of the observation for error-checking. Due to the need for automation, modification of the control file, downloading of met files, and generation of trajectories was handled using a modified and updated version of the R::SplitR package.

3. Results and Discussion

3.1. NO_2 and O_3 Dynamics over South Korean Coastal Land Sites

High frequency measurements from ground-based PSIs at the coastal land sites of Busan, Gwangju, Anmyeon, and Seoul (Figure 1, Table 1) provided detailed information on the spatial and temporal variability in atmospheric total column NO_2 and O_3 across areas characterized by different levels of anthropogenic influence in the South-east, Central-west, and North-west shorelines of South Korea.

The range and temporal dynamics in TCO_3 measured by the ground-based PSI network during May 2016, when the KORUS-OC campaign was held, were very similar across these four coastal sites (Figure 2, Table 2). Monthly average TCO_3 values were almost identical across sites, 314 DU (stdev = 19 DU), 311 DU (stdev = 19 DU), 315 DU (stdev = 17 DU), and 320 DU (stdev = 15 DU) at Busan, Gwangju, Anmyeon, and Seoul, respectively. Overall, TCO_3 varied by approximately 25% at each station, with most of this change captured by a quasi bi-weekly oscillation (13–15 days) that was clearly evident at all sites, and particularly, at Busan and Gwangju (Figure 2). Maxima in TCO_3 were measured on 4 and 17 May 2016, while minima were measured on 8–9 and 23–24 May 2016 (Figure 2). The quasi-biweekly oscillation is one of the major systems that affect tropical and subtropical weather and seasonal mean climate [41,42]. This quasi-biweekly mode in TCO_3 variation was also captured in satellite imagery from Aura-OMI (Figures 2 and 3).

Table 2. Comparison between satellite OMI and shipboard PSI TCO_3 and $TCNO_2$ measurements at coastal land PSI sites.

		OMI TCO_3	PSI TCO_3	%ΔTCO_3	OMI $TCNO_2$	PSI $TCNO_2$	%$\Delta TCNO_2$
Busan	Average	316 (±21)	314 (±19)	0.38%	0.32 (±0.17)	0.71 (±0.39)	−55.00%
1 May–31 May 2016	Range	281–358	279–357		0.14–0.90	0.09-3.05	
Gwangju	Average	315 (±20)	311 (±19)	1.17%	0.20 (±0.05)	0.31 (±0.13)	−37.01%
1 May–31 May 2016	Range	283–357	266–355		0.11–0.30	0.14–1.05	
Anmyeon	Average	322 (±21)	315 (±17)	2.15%	0.24 (±0.08)	0.27 (±0.14)	−11.37%
1 May–31 May 2016	Range	292–366	287–357		0.1–0.46	0.11–1.27	
Seoul	Average	323 (±22)	320 (±15)	1.15%	0.75 (±0.48)	1.01 (±0.64)	−25.45%
16 May–16 June 2016	Range	287–367	286–360		0.17–1.75	0.01–5.78	

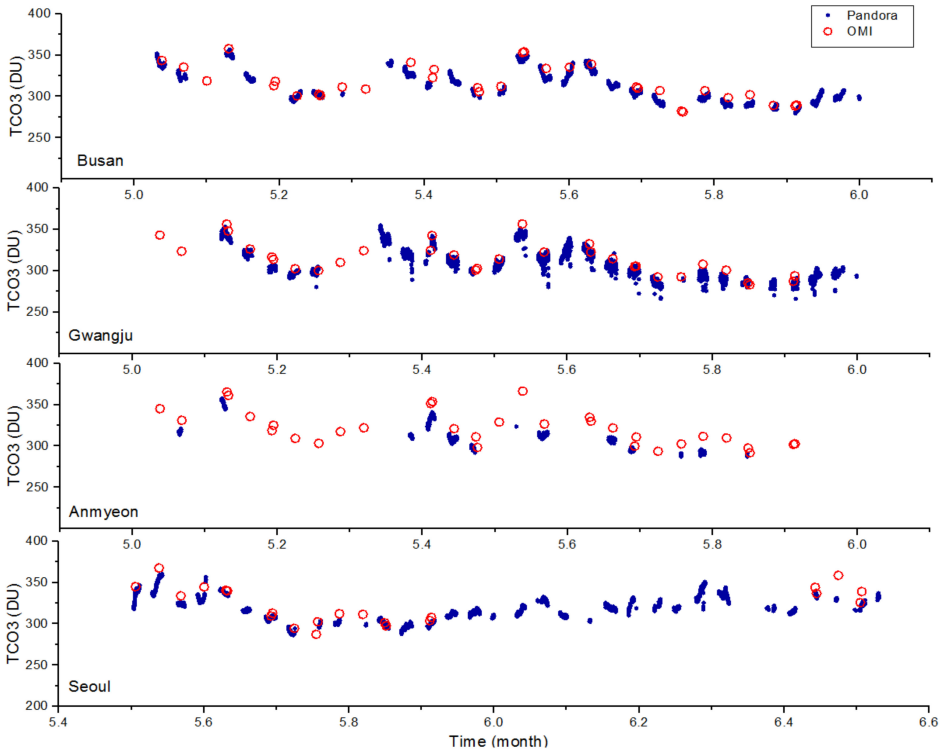

Figure 2. Spatial and temporal variability in TCO_3 (in DU) as observed by the ground-based PSI network (solid circles) at the four coastal sites of Busan, Gwangju, Anmyeon (1–31 May 2016) and Seoul (16 May–16 June 2016, due to no PSI-40 data availability in 1–16 May) (uncertainty in PSI TCO_3 data <2 DU). Satellite Aura-OMI overpass data is also shown (open circles). A quasi bi-weekly oscillation (12–14 days) affected temporal variability at all sites.

Satellite Aura-OMI retrievals of TCO_3 were in excellent agreement with the ground-based observations (Table 2), also showing 26% variability in TCO_3 (281-367 DU) over the study region during May 2016. The absolute percent difference (APD) in average TCO_3 retrieved by OMI and PSI was 0.38%, 1.17%., 2.15%, and 1.15% at Busan, Gwangju, Anmyeon, and Seoul, respectively, with OMI estimating slightly higher ozone values. OMI synoptic observations over South Korea highlighted the influence of large scale, eastward moving air masses on TCO_3 distributions (Figure 3). These results suggest that column O_3 dynamics over the South Korean peninsula were driven primarily by larger scale meteorological processes that can successfully be captured in the coarser satellite OMI imagery, as opposed to small scale heterogeneities and local emissions.

Contrary to TCO_3, total column NO_2 showed clear differences among coastal land sites and a strong influence of smaller scale processes and local emission sources. During May 2016, considerably

higher NO_2 pollution levels were measured at the coastal megacities of Seoul and Busan, with average $TCNO_2$ values of 1.01 DU (stdev = 0.64 DU) and 0.71 DU (stdev = 0.39 DU), respectively. $TCNO_2$ reached as high as 5.78 DU at Seoul and 3.05 DU at Busan (Table 2). Changes as large as 2.0 or 3 DU within 3 to 4 h were often recorded at these two stations (Figure 4), consistent with previous studies over longer time periods covering different seasons [19]. In the most rural areas of Gwangju and Anmyeon, $TCNO_2$ was significantly lower with average values of 0.31 DU (stdev = 0.13 DU) and 0.27 DU (stdev = 0.14 DU), but still reached as high as 1.05 DU and 1.27 DU, respectively, on certain days. Diurnal variability in NO_2 was not consistent across days or across stations, with maximum values occurring some days in the morning and some days in the early or late afternoon. A clear weekly pattern was observed at the coastal urban sites of Seoul and Busan (Figure 4). Minimum $TCNO_2$ values were consistently observed on Sundays and maximum values occurred mostly in the middle of the week, consistent with weekly cycles in anthropogenic NO_x emissions. This weekly pattern was much less pronounced at the less polluted Gwangju PSI site and absent in the more rural area of Anmyeon (Figure 4). These results agree with previous measurements in the Chesapeake Bay region, where a well-defined weekly behavior in $TCNO_2$ was captured with Pandora ground-based spectrometers at urban coastal locations [2].

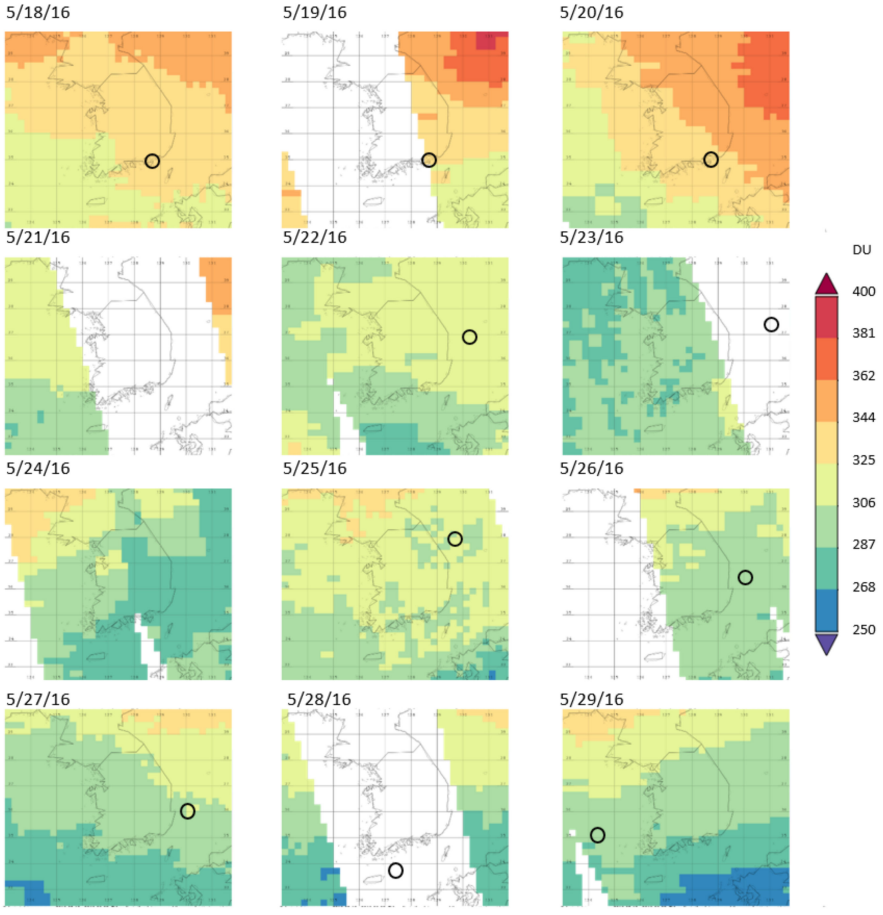

Figure 3. Satellite retrievals of spatial dynamics in total column ozone (TCO_3) from Aura OMI, during the KORUS OC campaign. Aura OMI data was not available during 30 May to 10 June due to satellite communication failure. The black circle indicates the location of the RV *Onnuri*.

Despite its coarse spatial resolution, satellite imagery from OMI highlighted the role of the two coastal megacities of Seoul and Busan as the major sources of anthropogenic NO_x emissions and hot spots of NO_2 over this coastal environment (Figure 5). Although not as well defined as in the high-frequency ground-based measurements, a weekly NO_2 pattern also emerged from the OMI

satellite imagery with $TCNO_2$ considerably less pronounced over the Seoul and Busan metropolitan areas on Sundays (22 May and 29 May, Figure 5). Still, due to its overpass at 13:30 local time, OMI cannot provide the full range in NO_2 pollution over South Korea, missing the early morning and/or late afternoon rush hour peaks in NO_x emissions often observed in urban regions, including Seoul and Busan. Tzortziou et al. [11] previously reported that during March 2012 to March 2013, OMI retrievals showed an average $TCNO_2$ of 0.5 DU (stdev = 0.21 DU) over Busan, and 0.79 DU (stdev = 0.45 DU) over Seoul, significantly underestimating NO_2 pollution levels compared to continuous measurements from ground-based instruments [11] (Figure 6). Similarly, during May 2016, the average $TCNO_2$ pollution observed over Busan and Seoul by OMI was 0.32 DU (stdev = 0.17 DU) and 0.75 DU (stdev = 0.48 DU), respectively. These NO_2 levels are 55% and 25% lower compared to average $TCNO_2$ amounts of 0.71 DU (stdev = 0.39 DU) and 1.01 DU (stdev = 0.64 DU) measured over the same period at Seoul and Busan, respectively, by the ground-based Pandora instruments. On May 18, the PSI at Geoje measured $TCNO_2$ in the range 0.3–0.9 DU, compared to 0.27 DU observed by OMI over the same location. In the less polluted coastal areas of Gwangju and Anmyeon, the absolute difference in average NO_2 was smaller, with OMI still underestimating $TCNO_2$ by 37% and 11%, respectively (Table 2). These differences between OMI and ground-based observations of $TCNO_2$ are to a large extent due to the coarser resolution of the satellite imagery and the time of the OMI overpass. Uncertainties in the OMI retrievals (e.g., NO_2 profile shape and surface reflectivity) would also be expected to contribute to the discrepancies between OMI and Pandora. Current research is focusing on reducing these uncertainties over land and over the ocean [43,44].

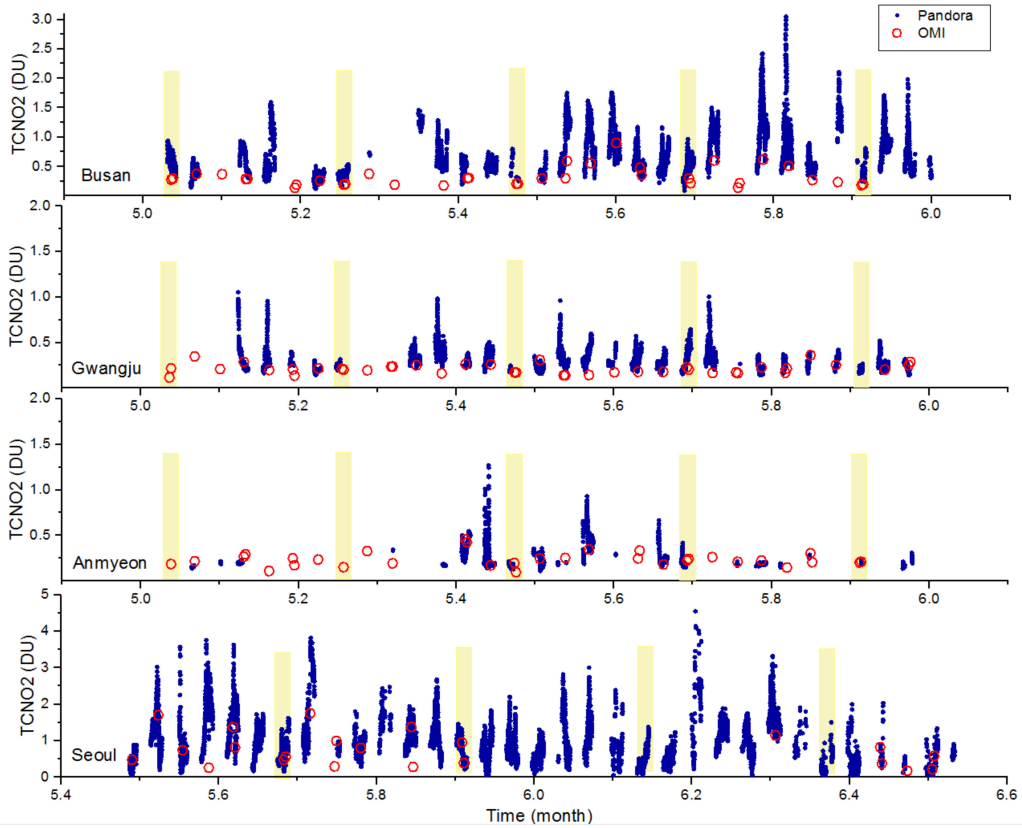

Figure 4. Spatial and temporal variability in $TCNO_2$ (in DU) as observed by the ground-based PSI network (solid circles) at the four coastal sites of Busan, Gwangju, Anmyeon (1–31 May 2016) and Seoul (16 May–16 June 2016) (uncertainty in PSI $TCNO_2$ data <0.2 DU). Satellite Aura-OMI overpass data is also shown (open circles). A weekly pattern, with $TCNO_2$ minima on Sundays (indicated by the shaded area), was more pronounced at the coastal urban sites of Seoul and Busan. The vertical extent is from the diurnal variation of $TCNO_2$.

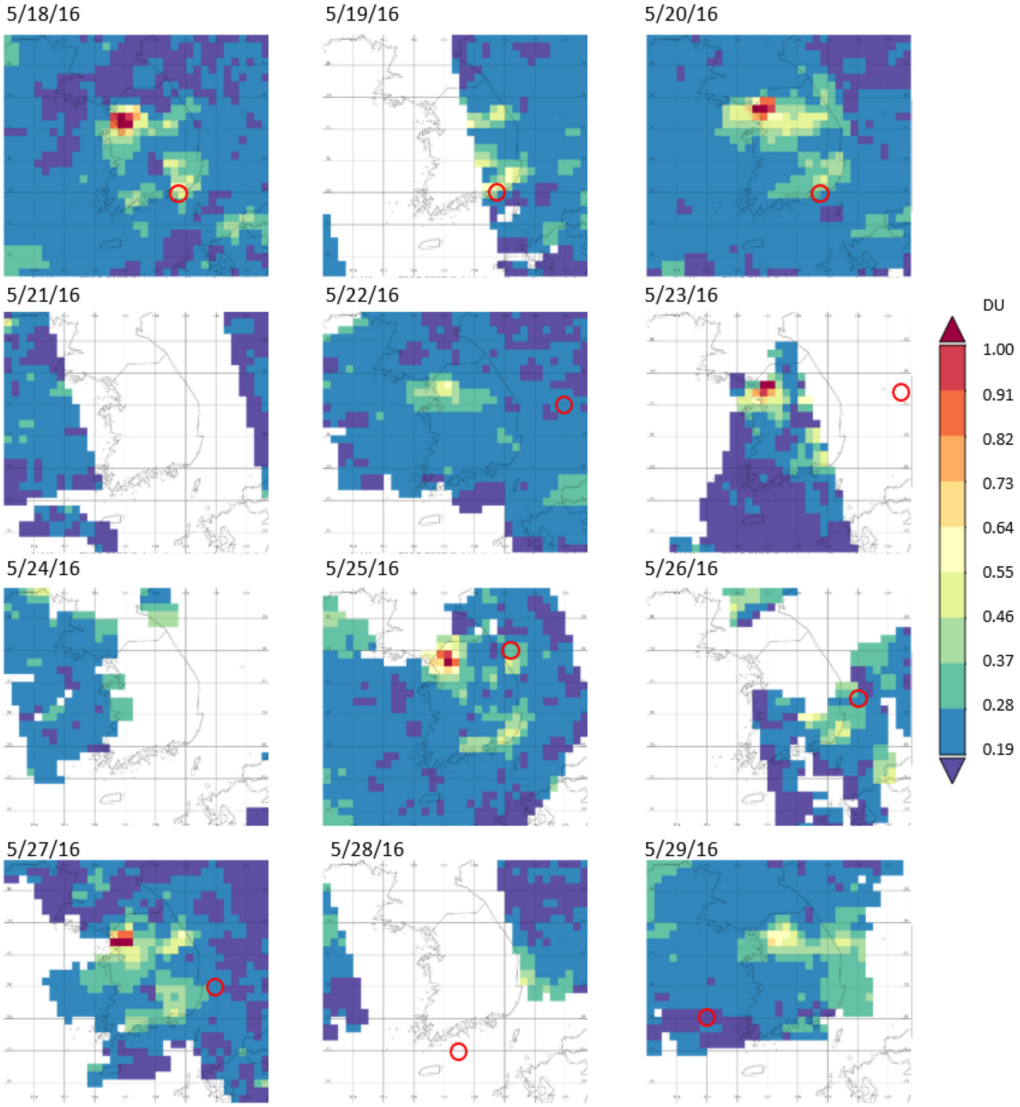

Figure 5. Satellite retrievals of spatial variability in total column nitrogen dioxide ($TCNO_2$) from Aura OMI, during the KORUS OC campaign. The red circle indicates the location of the RV *Onnuri*.

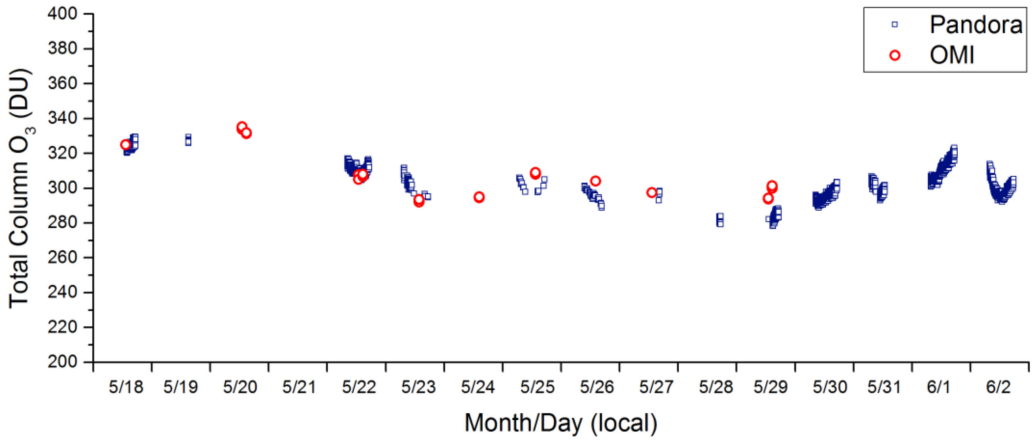

Figure 6. TCO_3 variability over the South Korean coastal waters, as measured by the shipboard PSI onboard RV *Onnuri* during the KORUS OC campaign (20 May–2 June, 2016) (blue open squares). Measurements during 18–20 May were collected at the coastal site of Geoje, more than 35 km from the city of Busan. Satellite Aura-OMI TCO_3 overpass data is also shown (red open circles).

3.2. NO_2 and O_3 Dynamics Over the South Korean Coastal Waters

Shipboard measurements from the RV *Onnuri* for the first time allowed us to capture the strong spatial and temporal variability in air quality over South Korean coastal waters. In agreement with measurements over the land, TCO_3 over the ocean varied by approximately 20% during the KORUS-OC campaign from a maximum value of 340 DU on 20 May to a minimum value of 278 DU on 28 May (Figure 6). Consistent with the quasi bi-weekly oscillation observed by the ground-based PSI network, relatively higher (>320 DU) ozone values were measured by the RV *Onnuri* during May 18–20, while TCO_3 remained relatively low (<300 DU) in the southern Korean Peninsula from 26 May to 30 May (Figure 6). Diurnal variability was small, with TCO_3 over the ocean changing by less than 7% (or, 22 DU) during any single day (Figure 6). These results are consistent with previous studies on TCO_3 temporal variability measured by Pandora instruments at various mid- to high-latitude sites in Europe and the US [2,11]. The average daily range in TCO_3 observed at urban and rural coastal sites along the Chesapeake Bay shorelines during the 2011 DISCOVER-AQ campaign ranged between 10 and 25 DU [2].

The range in TCO_3 observed over the ocean by the shipboard PSI was in remarkably good agreement with the coarser satellite observations from Aura-OMI (Figure 6). The mean APD between OMI and PSI observations (averaged over a 1 h window around the OMI overpass time) was 3%, while maximum APD was 7%. As discussed in the previous section, the larger scale synoptic observations from OMI revealed that these dynamics in TCO_3 over the ocean were to a large extent due to the passage of a front transporting air masses with total column ozone amount of 344–400 DU eastward and over the South Korean peninsula during 18 May to 21 May, while relatively low TCO_3 values, <320 DU, persisted over the study region later in May (Figure 3). The range in TCO_3 observed over the coastal ocean by the shipboard PSI was very consistent with ground-based observations at the coastal sites of Busan, Seoul, Gwangju, and Anmyeon, despite the >25 km distance of the RV *Onnuri* from the shoreline (Table 2).

Similar to measurements over the land, $TCNO_2$ over the South Korean coastal waters showed significantly stronger variability and heterogeneity compared to TCO_3. $TCNO_2$ varied by more than an order of magnitude, from 0.07 DU to 0.92 DU, both spatially and temporally during the campaign (Figure 7). The highest $TCNO_2$ values, as high as 0.92 DU, were measured at the beginning of the campaign (18–19 June 2016) at the KIOST dock at Geoje located at a distance of more than 35 km from the city of Busan. The amount and diurnal pattern in $TCNO_2$ measured by the shipboard PSI at the coastal site of Geoje on the afternoon of 18 May was in very good agreement with ground-based measurements in Busan (Figure 8), with a mean absolute difference of less than 0.22 DU (Figure 8). At both sites, $TCNO_2$ changed by more than 0.6 DU within a period of less than 3 h, with values as high as 0.9 DU at Geoje and 1.1 DU at Busan at 14:00 local time, decreasing to 0.3 DU at 17:00 local time. Satellite imagery from OMI, however, showed $TCNO_2$ of just 0.29 DU over Geoje and 0.55 DU over Busan, 0.5 and 0.6 DU lower, respectively, than coincident ($\pm$1 h from OMI overpass) PSI observations (Figure 8).

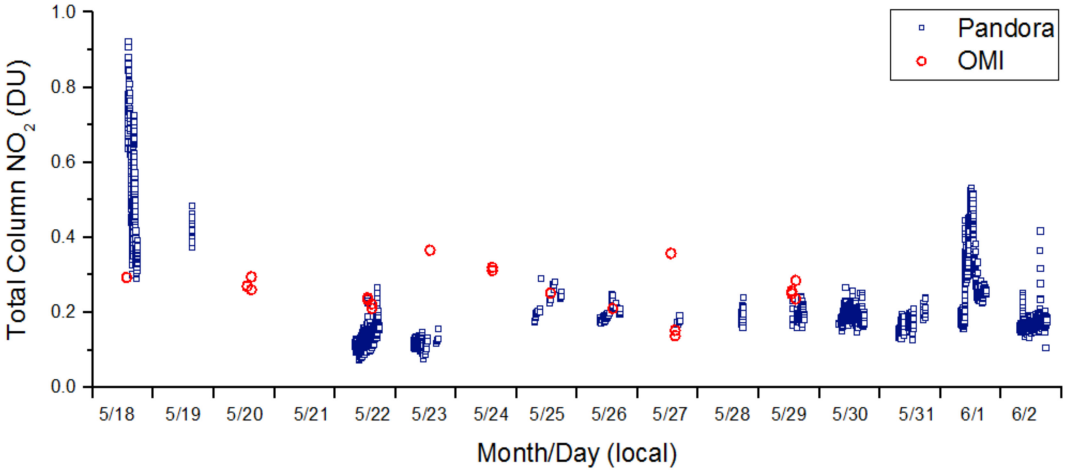

Figure 7. $TCNO_2$ variability over the coastal waters of Yellow Sea and East Sea, as measured by the shipboard PSI onboard RV *Onnuri* during the KORUS OC campaign (20 May–2 June, 2016) (blue open squares). Measurements during 18–20 May were collected at the coastal site of Geoje, more than 35 km from the city of Busan. Satellite Aura-OMI $TCNO_2$ overpass data is also shown (red open circles).

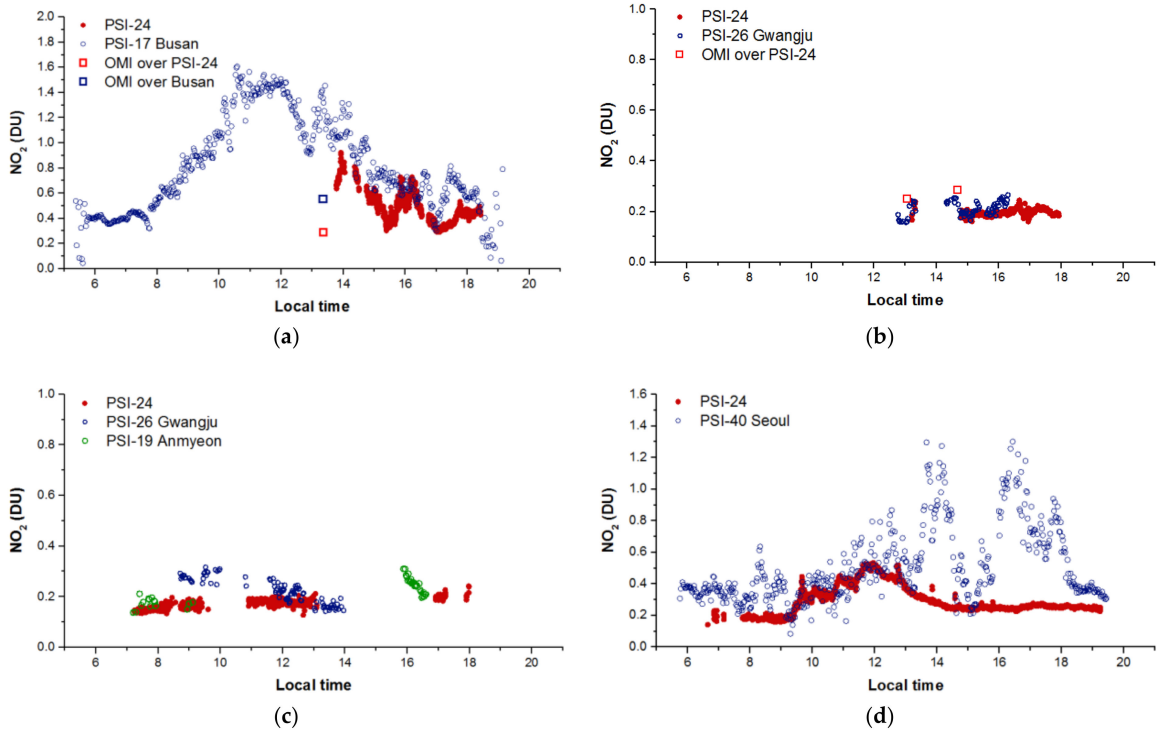

Figure 8. $TCNO_2$ measured by the shipboard PSI-24 (red solid circles) and the nearest ground-based PSI (blue open circles) (**a**) at Geoje, near the coastal megacity of Busan, on 18 May 2016; (**b**) offshore Gwangju on 29 May 2016; (**c**) offshore Gwangju and Anmyeon on 31 May 2016; and (**d**) offshore Seoul on 1 June 2016. The OMI $TCNO_2$ retrievals over RV *Onnuri* (red squares) and over Busan (blue square) are also shown for comparison. OMI measurements were not available for 29 May 2016 and 1 June 2016 due to a failure in the OMI instrument.

$TCNO_2$ was low off the northeast and southwest coasts of South Korea, ranging from 0.1 DU to 0.3 DU, and showing low diurnal variability. RV *Onnuri* was offshore the coastal city of Gwangju (at a distance of more than 150 km from the shoreline) on May 29, measuring column NO_2 in the range 0.16–0.24 DU with an average value of 0.2 DU (stdev = 0.01 DU) over the ocean compared to an average value of 0.25 DU (stdev = 0.06 DU) over the land at Gwangju. Relatively low $TCNO_2$ levels

were measured again over the ocean when the RV *Onnuri* was in the coastal waters between the coastal sites of Gwangju and Anmyeon on 31 May. $TCNO_2$ had an average value of 0.17 DU (stdev = 0.02 DU) over the water, consistent with measurements at Gwangju and Anmyeon showing $TCNO_2$ of 0.26 DU (stdev = 0.08 DU) and 0.22 DU (stdev = 0.05 DU), respectively (Figure 8). OMI was in good agreement with the shipboard PSI under these relatively low pollution levels, slightly overestimating $TCNO_2$ by 0.07 DU on average (Figure 7).

Significantly higher NO_2 levels were measured by the shipboard PSI on 1 June 2016, in the coastal waters offshore Seoul at a distance of more than 50 km from the shoreline (Figures 1 and 7). Column NO_2 showed strong diurnal variability, changing by 0.37 DU during a period of less than 3 h. Although between 8:00 and 10:00 local time $TCNO_2$ was relatively low (less than 0.2 DU), it suddenly exceeded 0.5 DU by local noon, decreasing again to <0.25 DU in the afternoon while RV *Onnuri* was almost stationary (Figure 8). Comparison of the shipboard PSI measurements with the ground-based PSI located near the city of Seoul showed some differences in $TCNO_2$ during the morning (up to 0.46 DU), very good agreement at around 12 noon when NO_2 peaked over the ocean, and differences as high as 1.0 DU (mean absolute difference of 0.4 DU) in the afternoon (Figure 8). These results suggest influence of different air masses and pollution sources at these two locations over the land and over the ocean. HYSPLIT backward trajectories, discussed in the next section, provided more insights into the impact of different air masses on NO_2 variability over the ocean.

3.3. Back-Trajectories of Atmospheric Pollution Plumes

Backward air parcel trajectories were simulated using HYSPLIT4 to determine the origin of air masses sampled by the shipboard PSI on RV *Onnuri* at Geoje and offshore the coastal sites of Gwangju, Anmyeon and Seoul (Figures 9 and 10). Results for 18 May 2016 (9:00 to 13:00 local time) showed that the air at 1500 m altitude over the coastal area of Geoje had gone through the city of Busan 2–3 h earlier, suggesting transport of pollution from this coastal megacity over the shipboard Pandora (Figure 9a). Similar results were obtained for back trajectories initiated hourly from 14:00 to 18:00 local time. This is consistent with the very good agreement in absolute $TCNO_2$ values and diurnal pattern measured at Geoje and the city of Busan that day (Figure 8a). Backward trajectories initiated over the location of RV *Onnuri* on 29 and 30 May also showed little diurnal variability, but in this case, results suggested southward and eastward transport, respectively, of marine air masses (Figure 9b,c). This is in agreement with the low and relatively constant $TCNO_2$ values measured over the ship on both days (Figure 8b,c).

Backward trajectories run for the location of RV *Onnuri* on 1 June 2016 highlighted the impact of transport of different air masses on diurnal NO_2 variability over the ocean. Trajectories initiated over the boat (1500 m AGL) before 10:00 local time, when $TCNO_2$ over the ocean was <0.25 DU, showed transport of air masses originating from a relatively rural area at the border of North and South Korea where $TCNO_2$ is typically relatively low (Figure 10). At 12:00 local time, however, the air mass reaching the RV *Onnuri* was coming mostly from the city of Seoul, coinciding with the peak in $TCNO_2$ observed over the ocean. After 12:00 local time, back trajectory simulations showed a gradual shift of the air mass pathway and origin from a more rural, lower $TCNO_2$ area south of Seoul (Figure 10), concurrent with a gradual decrease in the $TCNO_2$ measured by the shipboard PSI. At the same time, $TCNO_2$ amounts over the city of Seoul continued to rise, reaching maximum values later in the afternoon, associated with rush hour NO_x emissions in this urban area (Figure 8).

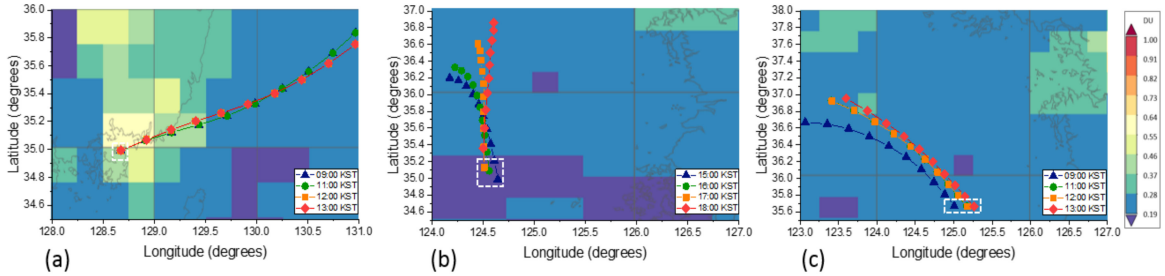

Figure 9. HYSPLIT4 simulated air parcel backward trajectories were used to determine the origin of air masses sampled by PSI-24 on RV *Onnuri* (**a**) at Geoje on 18 May 2016; (**b**) offshore Gwangju on 29 May 2016; and (**c**) offshore Anmyeon on 31 May 2016. Simulations were initiated at the ship location (area indicated by white square), at 1500 m AGL, and for different local times (indicated by different symbols). Satellite OMI $TCNO_2$ imagery (from same, or nearest, day) is superimposed on simulated trajectories for reference.

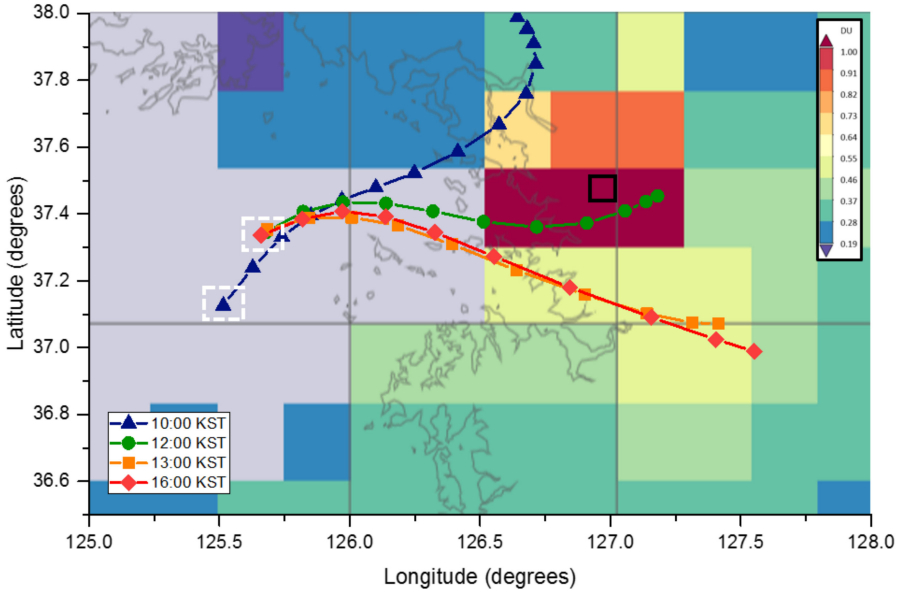

Figure 10. HYSPLIT4 simulated air mass backward trajectories for the locations of the RV *Onnuri* on 1 June 2016, when the research vessel was offshore the city of Seoul (indicated by black square). Simulations were initiated at the ship location (indicated by white square), at 1500 m AGL and 10:00, 12:00, 13:00 and 16:00 local times (KST). Satellite OMI $TCNO_2$ imagery (from, 27 May 2016, the nearest weekday when OMI data was available) is superimposed on the results for reference.

3.4. Implications of $TCNO_2$ Variability for Remote Sensing of Ocean Color Dynamics

The large spatial and temporal variability in $TCNO_2$ observed over this coastal environment has strong implications for remote sensing retrievals of ocean biogeochemical variability and ecological processes using ocean color observations. If this variability in $TCNO_2$ is not properly accounted for in satellite retrievals of ocean color, the decrease in the top of the atmosphere signal caused by NO_2 absorption will be incorrectly attributed to a lower reflectance from the ocean surface resulting in false variability in ocean properties [1,19]. Here, we used results from radiative transfer model calculations previously reported in the literature [19], and our measurements in South Korean coastal waters to examine the impact of observed variability in $TCNO_2$ on estimates of water remote sensing reflectance, R_{rs}, from space based platforms.

Previous studies using detailed radiative transfer calculations over optically thick coastal waters [1,19] showed that there is significant error in R_{rs} from unaccounted (temporal or spatial) NO_2 variability in atmospheric correction of ocean color observations. For 1 DU of unaccounted NO_2

the error is as large as 57–100% at 412 nm and 28–50% at 443 nm, for SZAs in the 30–60° range and for NO_2 homogeneously distributed within the first 2 km from the ground [19] (Figure 10). This error increases with increasing solar zenith and viewing angles due to (i) the increasing optical path, and (ii) the decreasing relative contribution of ocean water-leaving radiance to the TOA signal [19].

In South Korean coastal waters, $TCNO_2$ over the coastal area of Geoje ranged from 0.3 to 0.92 DU on 18 May 2016, compared to the OMI retrieval of 0.29 DU. This corresponds to a $TCNO_2$ uncertainty of 0.6 DU during the day, with some of the largest differences occurring at 14:00 and 16:00 local time corresponding to 25° and 50° SZA, respectively (Figure 11a). If unaccounted in atmospheric correction of coastal ocean color retrievals, the impact of such a change in $TCNO_2$ would be a false change in R_{rs}(412) by 37% during the day (Figure 11b). The error will be smaller for 443 nm, and almost negligible at 555 nm (Figure 11b), introducing an uncertainty not only in the absolute amount of R_{rs} but also in its spectral shape. Although a number of previous studies demonstrated the advantages of using green-red wavelengths for improved chlorophyll *a* retrievals in coastal waters [45–47], current operational retrievals for standard chlorophyll *a* products are still based on empirical relationships between chlorophyll *a* and R_{rs} at blue wavelengths (e.g., 443 and 490 nm) that are considerably affected by variability in atmospheric NO_2 [19]. Moreover, the spectral shape of R_{rs} in the spectral region affected by NO_2 absorption (i.e., <490 nm) is critical for discrimination of phytoplankton pigment assemblages in the ocean and for retrievals of the amount and quality of colored dissolved organic matter, both from current and future multi- and hyper-spectral satellite ocean color sensors [15–18,48].

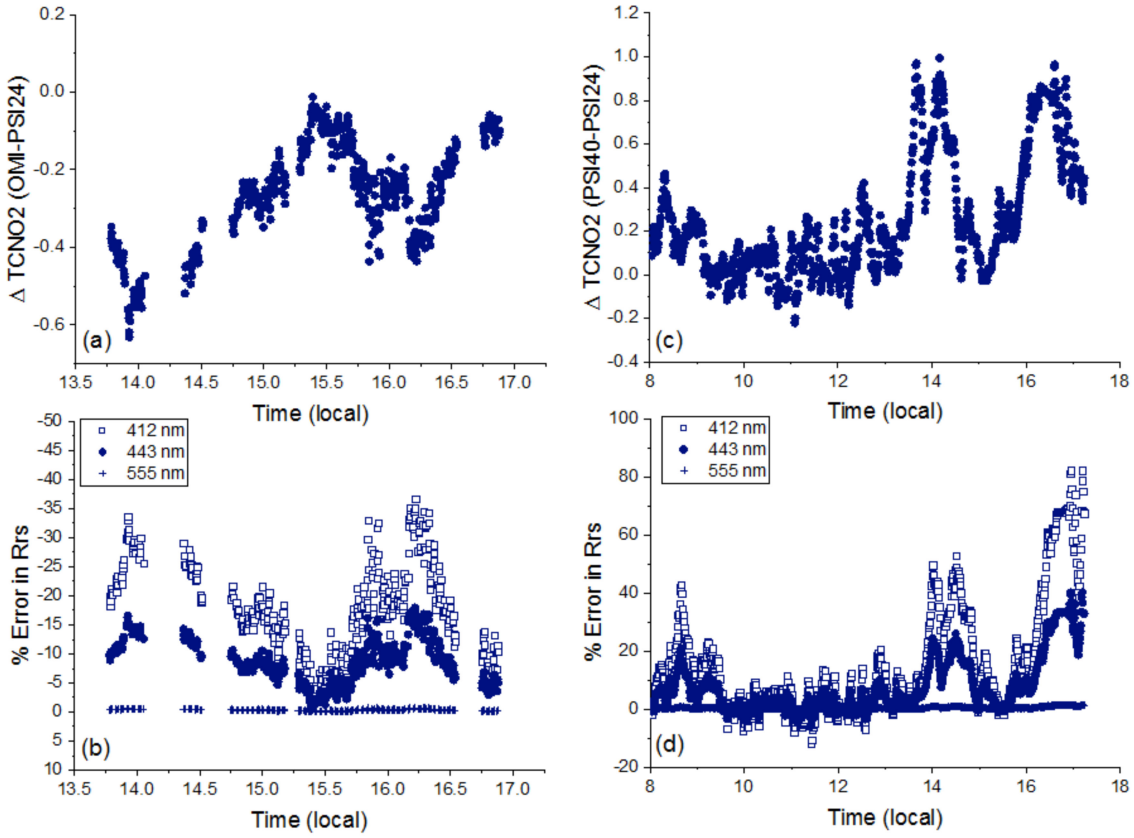

Figure 11. (**a**) Difference in $TCNO_2$ measured by OMI at 13:30 KST and PSI-24 at Geoje on 18 May 2016, and (**b**) resulting false diurnal variability (%) in retrieved R_{rs} due to unaccounted temporal variability in NO_2. (**c**) Difference in $TCNO_2$ measured by PSI-40 (Seoul ground-based site) and PSI-24 offshore Seoul on 1 June 2016, and (**d**) resulting false diurnal variability (%) in retrieved R_{rs} due to unaccounted variability in NO_2. Results are shown for R_{rs} at 412, 443 and 555 nm, for NO_2 homogeneously distributed within the first 2 km from the ground, and for varying SZA depending on time of day.

In the absence of information on the diurnal variability of $TCNO_2$ over the ocean (from shipboard or satellite platforms), the diurnal variability in $TCNO_2$ measured by ground-based instruments at nearby coastal land sites could be used as a reasonable alternative. However, our measurements in this coastal environment reveal that large differences often occur in the diurnal patterns of $TCNO_2$ over the land and over the adjacent ocean depending on meteorological processes and air-mass transport. In the case of measurements offshore Seoul, the amount and temporal variability in $TCNO_2$ over the ocean was in relatively good agreement (mean absolute difference of 0.09 DU) with measurements over the coastal city of Seoul at around 12:00 local time when the dominant source of air masses at 1500 m over the RV *Onnuri* was from the Seoul metropolitan area (Figure 10). However, considerably larger differences were observed in $TCNO_2$ amounts between the two locations earlier in the morning and later in the afternoon, as air masses from areas characterized by considerably lower NO_2 pollution were transported over the R/V *Onnuri* (Figure 10). Differences in $TCNO_2$ over the two locations in the morning were as high as 0.46 DU at 8:30 local time (SZA of 56°). Differences in the afternoon had an average value of 0.4 DU and were as large as 1 DU and 0.96 DU at around 14:00 and 16:30 local time or, 25° and 53° SZA, respectively (Figure 11c). Assuming homogeneous distribution of NO_2 within the first 1.5–2 km from the ground, such neglected changes in $TCNO_2$ would result in a false change in R_{rs}(412) of 43% in the morning and 82% in the afternoon, while changes in R_{rs}(443) would be 21% and 40%, respectively (Figure 11d). Such large errors in the amount and spectral shape of coastal ocean R_{rs} will, in turn, introduce large uncertainties in satellite retrievals of spatiotemporal changes in coastal water quality and coastal ocean biogeochemistry [19].

4. Conclusions

Variability in atmospheric aerosols and absorbing trace gases remains one of the largest sources of uncertainty for remote sensing of short-term (e.g., hourly to weekly) ocean processes, especially in coastal waters that are close to heavily polluted urban areas. A key objective of the Korea-US Ocean Color (KORUS OC) field campaign was to characterize atmospheric variability in the South Korean coastal waters in the context of the underlying optically complex waters to better understand future retrieval algorithm development needs for both polar orbiting and geostationary ocean color sensors [25].

Our measurements from a shipboard Pandora Spectrometer Instrument (PSI), specifically designed for direct-sun measurements from a moving platform, revealed for the first time the spatial and temporal dynamics that characterize total column (TC) O_3 and NO_2 amounts over the coastal waters of South Korea. In contrast to the relatively low (less than 20%) variability in column ozone, $TCNO_2$ over the ocean varied by more than an order of magnitude reaching values as high as 0.92 DU during the campaign. Temporal changes in TCO_3 mostly exhibited a quasi bi-weekly oscillation and spatial dynamics were driven primarily by larger scale meteorological processes and synoptic weather fronts that were captured successfully in the relatively coarse satellite imagery from the Aura Ozone Monitoring Instrument (OMI). Variability in $TCNO_2$, in contrast, was mostly affected by local anthropogenic emissions and highly dynamic air mass transport pathways. NO_2 emissions over the land considerably affected $TCNO_2$ dynamics over the ocean, but in complex ways, often resulting in very different temporal patterns between coastal land sites and offshore coastal waters. Although ground-based measurements showed a clear weekly pattern in NO_2 at coastal urban sites such as Seoul and Busan, with minima consistently observed on Sundays, this weekly cycle was not observed over the adjacent ocean. A combination of observations from high-frequency ground-based sensors, synoptic satellite imagery, and air-mass trajectory simulations explained the observed diurnal variability, which varied widely across the coastal ocean domain. A greater than 0.6 DU change in $TCNO_2$ over a period of less than 3 h in the coastal area of Geoje was mostly due to constant transport of air masses through the city of Busan, resulting in remarkably good agreement in the NO_2 diurnal variability observed at the two locations, despite their distance of more than 35 km. In the coastal waters offshore Seoul, transport of different air masses over the ocean caused $TCNO_2$ over the RV *Onnuri* to vary by almost

0.4 DU within a period of less than 3 h while the ship held its position at more than 50 km distance from the shoreline. Backward trajectory simulations initiated at the time of maximum NO_2 over the RV *Onnuri*, indicated transport from the Seoul metropolitan area, while a gradual decrease in NO_2 over the ocean 2 to 3 h later coincided with a gradual shift in air mass origin from a rural area south of Seoul characterized by considerably lower NO_2 levels. With coarse spatial resolution and an overpass at around 13:30 local time, OMI is not capable of detecting these small-scale, short-term changes in NO_2 observed by high-frequency shipboard remote-sensing sensors over these coastal waters. Observations from the higher spatial resolution (7 × 7 km) polar orbiting TROPOspheric Monitoring Instrument (TROPOMI) are expected to provide more information on spatial variability at a global scale, but will still be limited to one measurement per day temporal resolution. Future geostationary missions, such as NASA's TEMPO (Tropospheric Emissions: Monitoring Pollution), the Korean GEMS (Geostationary Environment Monitoring Spectrometer), and the European Sentinel-4, will provide a unique satellite capability to monitor the spatially and temporally varying $TCNO_2$ over coastal oceans.

If the observed variability in $TCNO_2$ is not properly accounted for in atmospheric correction retrievals of coastal ocean color, it will result in a false spatial or temporal variability in ocean biogeochemical properties and ecological processes. We found that uncertainties in $TCNO_2$ of 0.48 DU, similar to the difference between OMI and shipboard PSI retrievals in the coastal area of Geoje, would result in 37% uncertainty in $R_{rs}(412)$ and almost no change in $R_{rs}(555)$, introducing significant uncertainty in the spectral shape of ocean remote sensing reflectance. Uncertainties in NO_2 diurnal variability over the ocean, on the order of the difference in $TCNO_2$ measurements between Seoul and its offshore coastal waters on June 1 2016, would result in a false change in $R_{rs}(412)$ and $R_{rs}(443)$ by more than 80% and 40%, respectively, during the day. The resulting errors in R_{rs} subsequently introduce a false variability in retrievals of ocean biogeochemical variables from space, which would be practically impossible to distinguish from real spatiotemporal patterns in coastal ocean dynamics without nearly coincident measurements of NO_2 over the area of interest [12,13,19]. These results are consistent with recent studies by Pahlevan et al. [20] showing that even 10% uncertainty in $TCNO_2$ would introduce significant, and time-dependent, uncertainties in retrievals of R_{rs} at 412–440 nm in South Korean coastal waters, inhibiting the ability of satellite ocean color sensors to retrieve information on ocean dynamics and biological responses to short-term biogeochemical and physical forcing.

Our measurements demonstrated that variability in TCO_3 over the South Korean coastal waters is mostly driven by large-scale, synoptic features that can accurately be captured by coarser polar orbiting satellite sensors. Short-term (i.e., diurnal to weekly) and small-scale variability in $TCNO_2$ needs to be taken into consideration when attempting to retrieve short-term coastal ocean processes from satellite ocean color imagery. This is necessary to avoid misinterpreting atmospheric variability as diurnal changes, weekly cycles, or spatial gradients in ocean composition. Since current model predictions of trace gas variability are not adequate for deriving atmospheric corrections, more measurements from shipboard platforms are needed across inland and coastal aquatic environments. Improved modeling is essential for the prediction of atmospheric trace gas variability and its impacts on satellite retrievals of highly dynamic biogeochemical and ecological processes in nearshore ecosystems.

Author Contributions: M.T. designed and directed this study, conducted the analysis, and wrote the original manuscript. J.H., O.P., B.L., N.A., and R.S., contributed to the collection of field measurements, air-mass trajectory simulations, and analysis of results. L.L. contributed to the satellite data analysis. All authors contributed to manuscript preparation and revision.

Funding: This work was supported under the National Aeronautics and Space Administration (NASA) KORUS-OC/AQ field campaign (Grant: NASA. NNX16AD60G), with additional support from grants NASA.NNX13AL86G, NASA.NNX15AB84G, NASA. NNX16AQ53A, and NOAA Grant NA16SEC4810008.

Acknowledgments: The authors would like to thank Antonio Mannino, Jhoon Kim, Jay Al-Saadi, the KORUS OC/AQ teams, and the GEO-CAPE Ocean Science Working Group for their support during the KORUS OC/AQ field campaign. The authors would also like to thank Xinrong Ren, Mark Cohen, and Alice Crawford from NOAA Air Resources Laboratory (ARL) for their guidance with the HYSPLIT4 trajectory analysis and comparison with field observations.

Conflicts of Interest: The authors declare no conflicts of interest

References

1. Herman, J.; Cede, A.; Spinei, E.; Mount, G.; Tzortziou, M.; Abuhassan, N. NO_2 Column Amounts from Ground-based Pandora and MFDOAS Spectrometers using the Direct-Sun DOAS Technique: Intercomparisons and Application to OMI Validation. *JGR Atmos.* **2009**, *114*. [CrossRef]
2. Tzortziou, M.; Herman, J.R.; Cede, A.; Loughner, C.P.; Abuhassan, N.; Naik, S. Spatial and temporal variability of ozone and nitrogen dioxide over a major urban estuarine ecosystem. *J. Atmos. Chem.* **2013**. [CrossRef]
3. Goldberg, D.L.; Loughner, C.P.; Tzortziou, M.; Stehr, J.W.; Pickering, K.E.; Marufu, L.T.; Dickerson, R.R. Higher surface ozone concentrations over the Chesapeake Bay than over the adjacent land: Observations and models from the DISCOVER-AQ and CBODAQ campaigns. *Atmos. Environ.* **2014**, *84*, 9–19. [CrossRef]
4. Loughner, C.P.; Tzortziou, M.; Shroder, S.; Pickering, K.E. Enhanced dry deposition of nitrogen pollution near coastlines: A case study covering the Chesapeake Bay estuary and Atlantic Ocean coastline. *J. Geophys. Res. Atmos.* **2016**, *121*, 14–221. [CrossRef]
5. Tie, X.; Geng, F.; Peng, L.; Gao, W.; Zhao, C. Measurement and modeling of O3 variability in Shanghai, China: Application of the WRF-Chem model. *Atmos. Environ.* **2009**, *43*, 4289–4302. [CrossRef]
6. Kanakidou, M.; Mihalopoulos, N.; Kindap, T.; Im, U.; Vrekoussis, M.; Dermitzaki, E.; Gerasopoulos, E.; Unal, A.; Kocak, M.; Markakis, K.; et al. Megacities as hot spots of air pollution in the East Mediterranean. *Atmos. Environ.* **2011**, *45*, 1223–1235. [CrossRef]
7. Von Glasow, R.; Jickells, T.D.; Baklanov, A.; Carmichael, G.R.; Church, T.M.; Gallardo, L.; Hughes, C.; Kanakidou, M.; Liss, P.S.; Mee, L.; et al. Megacities and large urban agglomerations in the coastal zone: Interactions between atmosphere, land, and marine ecosystems. *Ambio* **2013**, *42*, 13–28. [CrossRef] [PubMed]
8. Stauffer, R.; Thompson, A.; Martins, D.K.; Clark, R.D.; Loughner, C.P.; Delgado, R.; Berkoff, T.A.; Gluth, E.C.; Dickerson, R.R.; Stehr, J.W.; et al. Bay Breeze Influence on Surface Ozone at Edgewood, MD, during July 2011. *J. Atmos. Chem.* **2012**. [CrossRef] [PubMed]
9. Loughner, C.P.; Tzortziou, M.; Follette-Cook, M.; Pickering, K.E.; Goldberg, D.; Satam, C.; Weinheimer, A.; Crawford, J.H.; Knapp, D.J.; Montzka, D.D.; et al. Impact of bay breeze circulations on surface air quality and boundary layer export. *J. Appl. Meteorol. Climatol.* **2014**, *53*, 1697–1713. [CrossRef]
10. Ahmad, Z.; McClain, C.R.; Herman, J.R.; Franz, B.A.; Kwiatkowska, E.J.; Robinson, W.D.; Bucsela, E.J.; Tzortziou, M. Atmospheric correction for NO_2 absorption in retrieving water-leaving reflectances from the SeaWiFS and MODIS measurements. *Appl. Opt.* **2007**, *46*, 6504–6512. [CrossRef] [PubMed]
11. Tzortziou, M.; Herman, J.R.; Cede, A.; Abuhassan, N. High precision, absolute total column ozone measurements from the Pandora spectrometer system: Comparisons with data from a Brewer double monochromator and Aura OMI. *J. Geophys. Res.* **2012**, *117*, D16303. [CrossRef]
12. Fishman, J.; Iraci, L.T.; Al-Saadi, J.; Chance, K.; Chavez, F.; Chin, M.; Coble, P.; Davis, C.; DiGiacomo, P.M.; Edwards, D.; et al. The United States' Next Generation of Atmospheric Composition and Coastal Ecosystem Measurements: NASA's Geostationary Coastal and Air Pollution Events (GEO APE) Mission. *Bull. Am. Meteorol. Soc.* **2012**. [CrossRef]
13. Salisbury, J.; Davis, C.; Erb, A.; Chuanmin, H.; Gatebe, C.; Jordan, C.; Lee, Z.; Mannino, A.; Mouw, C.B.; Schaaf, C.; et al. Coastal observations from a New Vantage Point: The NASA GEO-CAPE ocean mission. *EOS Trans. J.* **2016**, *97*. [CrossRef]
14. Mobley, C.D.; Werdell, J.; Franz, B.; Ahmad, Z.; Bailey, S. *Atmospheric Correction for Satellite Ocean Color Radiometry*; A Tutorial and Documentation NASA Ocean Biology Processing Group, NASA Goddard Space Flight Center: Greenbelt, MD, USA, 2016; pp. 1–73.
15. O'Reilly, J.E.; Maritorena, S.; Siegel, D.A.; O'Brien, M.C.; Toole, D.; Mitchell, B.G.; Kahru, M.; Chavez, F.P.; Strutton, P.; Cota, G.F.; et al. *Ocean Color Chlorophyll a Algorithms for SeaWiFS, OC2, and OC4: Version 4*; SeaWiFS Postlaunch Calibration and Validation Analyses, Part 3, NASA Tech. Memo. 2000-206892; NASA Goddard Space Flight Center: Greenbelt, MD, USA, 2000; Volume 11.
16. Carder, K.L.; Chen, F.R.; Lee, Z.; Hawes, S.K.; Cannizzaro, J.P. *Case 2 Chlorophyll-a MODIS Ocean Science Team Algorithm Theoretical Basis Document*; Version 6, ATBD; 2002.

17. Mannino, A.; Russ, M.E.; Hooker, S.B. Algorithm development for satellite-derived distributions of DOC and CDOM in the U.S. Middle Atlantic Bight. *J. Geophys. Res.* **2008**, C07051. [CrossRef]
18. Cao, F.; Tzortziou, M.; Hu, C.; Mannino, A.; Fichot, C.G.; Del Vecchio, R.; Najjar, R.G.; Novak, M. Remote Sensing retrievals of colored dissolved organic matter and dissolved organic carbon dynamics in North American eutrophic estuaries and their margins. *Remote Sens. Environ.* **2018**, *205*, 151–165. [CrossRef]
19. Tzortziou, M.; Herman, J.R.; Ahmad, Z.; Loughner, C.P.; Abuhassan, N.; Cede, A. Atmospheric NO_2 Dynamics and Impact on Ocean Color Retrievals in Urban Nearshore Regions. *J. Geophys. Res.-Oceans* **2008**, C07051. [CrossRef]
20. Pehlevan, N.; Ahn, J.; Jordan, C.E.; Tzortziou, M. Measurement requirements of atmospheric parameters for diurnal remote-sensing reflectance products. In Proceedings of the Abstract # 315585, 2018 Ocean Sciences Meeting, Portland, Oregon, 11–16 February 2018.
21. Al-Saadi, J.; Carmichael, G.; Crawford, J.; Emmons, L.; Kim, S.; Song, C.-K.; Chang, L.-S.; Lee, G.; Kim, J.; Park, R. *KORUS-AQ: An International Cooperative Air Quality Field Study in Korea*; White Paper; 2014.
22. Akimoto, H. Global air quality and pollution. *Science* **2003**, *302*, 1716–1719. [CrossRef] [PubMed]
23. Richter, A.; Burrows, J.P.; Nüß, H.; Granier, C.; Niemeier, U. Increase in tropospheric nitrogen dioxide over China observed from space (and Supplementary Discussion on: Error estimates for changes in tropospheric NO_2 columns as derived from satellite measurements). *Nature* **2005**, *437*, 129–132. [CrossRef] [PubMed]
24. Lin, J.; Pan, D.; Davis, S.J.; Zhang, Q.; He, K.; Wang, C.; Streets, D.G.; Wuebbles, D.J.; Guan, D. China's international trade and air pollution in the United States. *Proc. Natl. Acad. Sci. USA* **2014**, *111*, 1736–1741. [CrossRef] [PubMed]
25. Park, Y.; Ahn, Y.-H.; Salisbury, J.; Mannino, A.; The GEO-CAPE Ocean Color Science Working Group. *Risk Reduction Measurements for GEO-CAPE: A US-Korea Joint Field Campaign (US-Korea JFC) in the East Sea and Yellow Sea*; White Paper; 2016.
26. Pandey, S.K.; Kim, K.H.; Chung, S.Y.; Cho, S.J.; Kim, M.Y.; Shon, Z.H. Long-term study of NO_x behavior at urban roadside and background locations in Seoul, Korea. *Atmos. Environ.* **2008**, *42*, 607–622. [CrossRef]
27. Guttikunda, S.K.; Tang, Y.; Charmichael, G.R.; Kurata, G.; Pan, L.; Streets, D.G.; Woo, J.-H.; Thongboonchoo, N.; Fried, A. Impacts of Asian megacity emissions on regional air quality during spring 2001. *J. Geophys. Res.* **2005**, *110*, D20301. [CrossRef]
28. Herman, J.; Spinei, E.; Fried, A.; Kim, J.; Kim, J.; Kim, W.; Cede, A.; Abuhassan, N.; Segal-Rozenhaimer, M. NO_2 and HCHO measurements in Korea from 2012 to 2016 from Pandora spectrometer instruments compared with OMI retrievals and with aircraft measurements during the KORUS-AQ campaign. *Atmos. Meas. Tech.* **2018**, *11*, 4583–4603. [CrossRef]
29. Levelt, P.F.; van den Oord, G.H.; Dobber, M.R.; Malkki, A.; Visser, H.; de Vries, J.; Stammes, P.; Lundell, J.O.; Saari, H. The Ozone Monitoring Instrument. *IEEE Trans. Geosci. Remote Sens.* **2006**, *44*, 1093–1101. [CrossRef]
30. Boersma, K.F.; Eskes, H.J.; Veefkind, J.P.; Brinksma, E.J.; van der A, R.J.; Sneep, M.; van den Oord, G.H.J.; Levelt, P.F.; Stammes, P.; Gleason, J.F.; et al. Near-real time retrieval of tropospheric NO_2 from OMI. *Atmos. Chem. Phys.* **2007**, *7*, 2103–2118. [CrossRef]
31. Lamsal, L.N.; Krotkov, N.A.; Celarier, E.A.; Swartz, W.H.; Pickering, K.E.; Bucsela, E.J.; Gleason, J.F.; Martin, R.V.; Philip, S.; Irie, H.; et al. Evaluation of OMI operational standard NO_2 column retrievals using in situ and surface-based NO2 observations. *Atmos. Chem. Phys.* **2014**, *14*, 11587–11609. [CrossRef]
32. Dobber, M.; Kleipool, Q.; Dirksen, R.; Levelt, P.; Jaross, G.; Taylor, S.; Kelly, T.; Flynn, L.; Leppelmeier, G.; Rozemeijer, N. Validation of Ozone Monitoring Instrument level 1b data products. *J. Geophys. Res.* **2008**, *113*, D15S06. [CrossRef]
33. Draxler, R.R.; Hess, G.D. *Description of the HYSPLIT_4 Modeling System*; NOAA Tech. Memo. ERL ARL-224; NOAA Air Resources Laboratory: Silver Spring, MD, USA, 1997; 24p.
34. Draxler, R.R.; Hess, G.D. An overview of the HYSPLIT_4 modeling system of trajectories, dispersion, and deposition. *Aust. Meteor. Mag.* **1998**, *47*, 295–308.
35. Challa, V.S.; Jayakumar, I.; Baham, J.M.; Hughes, R.; Patrick, C.; Young, J.; Rabbarison, M.; Swanier, S.; Hardy, M.G.; Anjaneyulu, Y. Sensitivity of atmospheric dispersion simulations by HYSPLIT to the meteorological predictions from a mesoscale model. *Environ. Fluid Mech.* **2008**, *8*, 367–387. [CrossRef]
36. Wang, M.; Shi, W.; Jiang, L. Atmospheric correction using near-infrared bands for satellite ocean color data processing in the turbid western Pacific region. *Opt. Express* **2012**, *20*, 741–753. [CrossRef] [PubMed]

37. Yerramilli, A.; Dodla, V.B.R.; Challa, V.S.; Myles, L.; Pendergrass, W.R.; Vogel, C.A.; Dasari, H.P.; Tuluri, F.; Baham, J.M.; Hughes, R.L.; et al. An integrated WRF/HYSPLIT modeling approach for the assessment of PM2.5 source regions over the Mississippi Gulf Coast region. Air Quality. *Atmos. Health* **2012**, *5*, 401–412. [CrossRef] [PubMed]
38. Stein, A.F.; Draxler, R.R.; Rolph, G.D.; Stunder, B.J.; Cohen, M.D.; Ngan, F. NOAA's HYSPLIT atmospheric transport and dispersion modeling system. *Bull. Am. Meteorol. Soc.* **2015**, *96*, 2059–2077. [CrossRef]
39. Draxler, R.R. *HYSPLIT4 User's Guide*; NOAA Tech. Memo. ERL ARL-230; NOAA Air Resources Laboratory: Silver Spring, MD, USA, 1999.
40. Su, L.; Yuan, Z.; Fung, J.C.H.; Lau, A.K.H. A comparison of HYSPLIT backward trajectories generated from two GDAS datasets. *Sci. Total Environ.* **2015**, *506–507*, 527–537. [CrossRef] [PubMed]
41. Kikuchi, K.; Wang, B. Global perspective of the quasi-biweekly oscillation. *J. Clim.* **2009**, *22*, 1340–1359. [CrossRef]
42. Madhu, V. Madden Julian Oscillations in Total Column Ozone, Air Temperature and Surface Pressure Measured over Cochin during Summer Monsoon 2015. *Open J. Mar. Sci.* **2016**, *6*, 270–282. [CrossRef]
43. Vasilkov, A.; Qin, W.; Krotkov, N.; Lamsal, L.; Spurr, R.; Haffner, D.; Joiner, J.; Yang, E.-S.; Marchenko, S. Accounting for the effects of surface BRDF on satellite cloud and trace-gas retrievals: A new approach based on geometry-dependent Lambertian equivalent reflectivity applied to OMI algorithms. *Atmos. Meas. Tech.* **2017**, *10*, 333–349. [CrossRef]
44. Vasilkov, A.; Yang, E.-S.; Marchenko, S.; Qin, W.; Lamsal, L.; Joiner, J.; Krotkov, N.; Haffner, D.; Bhartia, P.K.; Spurr, R. A cloud algorithm based on the O2-O2 477 nm absorption band featuring an advanced spectral fitting method and the use of surface geometry-dependent Lambertian-equivalent reflectivity. *Atmos. Meas. Tech.* **2018**, *11*, 4093–4107. [CrossRef]
45. Gitelson, A.A.; Schalles, J.F.; Hladik, C.M. Remote chlorophyll-a retrieval in turbid, productive estuaries: Chesapeake Bay case study. *Remote Sens. Environ.* **2007**, *109*, 464–472. [CrossRef]
46. Tzortziou, M.; Subramaniam, A.; Herman, J.; Gallegos, C.; Neale, P.; Harding, L. Remote sensing reflectance and inherent optical properties in the Mid Chesapeake Bay. *Estuarine Coast. Shelf Sci.* **2007**, *72*, 16–32. [CrossRef]
47. Le, C.; Hu, C.; Cannizzaro, J.; English, D.; Muller-Karger, F.; Lee, Z. Evaluation of chlorophyll-a remote sensing algorithm for an optically complex estuary. *Remote Sens. Environ.* **2013**, *129*, 75–89. [CrossRef]
48. Torrecilla, E.; Stramski, D.; Reynolds, R.A.; Millán-Núñez, E.; Piera, J. Cluster analysis of hyperspectral optical data for discriminating phytoplankton pigment assemblages in the open ocean. *Remote Sens. Environ.* **2011**, *115*, 2578–2593. [CrossRef]